A Fully 3D Atomistic Quantum Mechanical Study on Random Dopant Induced Effects in 25nm MOSFETs

Xiang-Wei Jiang, Hui-Xiong Deng, Jun-Wei Luo, Shu-Shen Li, Jian-Bai Xia, and Lin-Wang Wang*

***Abstract*— We present a fully 3D atomistic quantum mechanical simulation for nanometered MOSFET using a coupled Schrödinger equation and Poisson equation approach. Empirical pseudopotential is used to represent the single particle Hamiltonian and linear combination of bulk band (LCBB) method is used to solve the million atom Schrödinger's equation. We studied gate threshold fluctuations and threshold lowering due to the discrete dopant configurations. We compared our results with semiclassical simulation results. We found quantum mechanical effects increase the threshold fluctuation while decreases the threshold lowering. The increase of threshold fluctuation is in agreement with previous study based on approximated density gradient approach to represent the quantum mechanical effect. However, the decrease in threshold lowering is in contrast with the previous density gradient calculations.**

***Index Terms*— Dopant fluctuation, MOSFETs, 3D, threshold, LCBB, quantum mechanical.**

I. Introduction

ACCORDING to the roadmap of the semiconductor Industry Association [1], MOSFET (metal oxide semiconductor field transistor) channel length will scale down to sub-25nm at the end of this decade. In such nanosized devices, quantum mechanical effects play a big role in determining the properties of the system. The new quantum mechanical features, like the fact that the electron mean free path is larger than the device dimensions and the single quantum state levels, can be used to enhance device performance and form new functionalities [2], [3], [4]. On the other hand, as the size reduces, new obstacles emerge [3], [5], like the short channel effects, source/drain off-state quantum tunneling current, barrier current leakage and single dopant random fluctuation [6]. The single dopant random fluctuation poses a fundamental challenge to the device down scaling. How to reduce this fluctuation is an intensely researched topic. In this paper, we present an atomistic simulation to study this fluctuation effect, especially to investigate whether quantum mechanical effects enhance or reduce this random fluctuation, and what is the cause of the fluctuation change.

Xiang-Wei Jiang and Hui-Xiong Deng are with the Institute of Semiconductor of Chinese Academy of Science (ISCAS) pursuing the Ph.D. degree in semiconductor physics, under the supervision of Prof. Shu-Shen Li. Shu-Shen Li is the director of the State Key Laboratory for Superlattices and Microstructures, ISCAS. Jun-Wei Luo is now with the National Renewable Energy Laboratory, Colorado, USA. Jian-Bai Xia is now with the ISCAS, and he is also an academician of Chinese Academy of Science. Lin-Wang Wang is with the Computational Research Division, Lawrence Berkeley National Laboratory, Berkeley, CA. Author to whom correspondence should be addressed: electronic mail: lwwang@lbl.gov

In recent years, various kind of simulation approaches have been developed to simulate the MOSFET devices. Most noticably, these include Drift-Diffusion Model and Density-Gradient Model [7]. They are based on Bolzmann equation and local semi-classical density of state calculations. The local density of state calculation is not valid in true quantum mechanical regime. A much better approach is to solve the electron eigenstates and occupied carrier densities based on the carrier's Schrödinger's equation, and solve the potential selfconsistently with the carrier charge density via a Poisson equation. This Schrödinger-Poisson equation approach has been used to study MOSFET devices for continuous doping model, and the random dopant fluctuation in approximated model [8]. However, only simple effective mass Schrödinger's equation was used, which might not be very accurate when the variation of the potential is sharp, as in the perpendicular direction of the gate. Recently, we have developed an Schrödinger-Poisson equation approach based on empirical pseudopotential method (EPM) for the electron Schrödinger's equation [9]. The atomistic EPM description is much more accurate than the effective mass description for the electronic structure, and its atomistic feature makes it natural to study the dopant fluctuation effects. This approach use the linear combination of bulk band (LCBB) method [10], [11] to calculate the electron structure, which enables it to solve million atom systems, hence to simulate 3D MOSFET model. Here, we will use this approach to study the dopant fluctuation effects in a nanometered MOSFET.

The single dopant random fluctuation effect was first recongized by Mead and Hoeneisen in the 1970s [12]. It has been intensely studied in the last 10 years. As the device dimension scales down to nanosize, the number and position of the dopant atoms in the sensitive channel region will vary among devices. As a result, the macroscopically same devices become microscopically different, and demonstrate different device characteristics, like in the I/V curves and gate threshold voltages. This is a major challenge for device industry. It is possible that this alone will stop the device down scaling before the other technical difficulties take into effects. These random dopant fluctuation effects have been studied theoretically by different simulation approaches, the most well known one of which is the Density-Gradient simulation presented by Asenov's group [13]. This generalized Density Gradient method introduces an gradient dependent free energy potential term in the current diffusion equation to represent the quantum mechanical effects [14], [15]. Its validity has been checked by comparing its results with effective mass

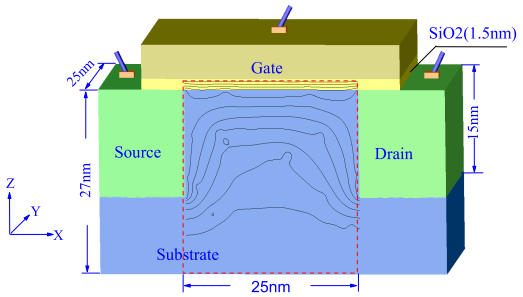

Fig. 1. (Color online) Geometry of the MOSFET structure along with electrostatic potential contour lines with $V_{ds} = 0.0V$ and $V_g = 2.0V$ in one of the random doping cases. The average doping density in substrate (p type) is $10^{19}cm^{-3}$. Schrödinger equation and Poisson equation are solved self-consistently in the dashed line box.

Schrödinger-Poisson equation results for simple systems like 2D device models. It is found that [13] one has to use a fitting parameter as the electron effective mass in order to reproduce the Schrödinger-Poisson equation results. This exemplifies the short comings of such approximated approaches. It is not clear how such equations with fitted parameters from simple systems (e.g, continuous doping models and 2D systems) will play out in actual 3D simulations. It is thus desirable to do a direct Schrödinger-Poisson equation simulation for the same physical problem. Further more, in our case the Schrödinger's equation is based on EPM, thus much more accurate than the simple effective mass model

II. Simulation Approach

The MOSFETs we simulated are of n-carrier reverse type and have 25 nm channel length with oxide thickness $t_{ox} = 1.5nm$. In such a device, the nominal doping is p-type, with the average acceptor concentration in the channel region as $N_A = 1.0 \times 10^{19}cm^{-3}$. Fig.1 shows the geometry of the MOSFETs we simulated. Schrödinger equation and Poisson equation were solved in the region included in the dashed line box. We take 27 nm in the z direction for the simulated box. Thus, there are 0.85 million atoms in the simulated system. Fig.1 also shows the electrostatic potential distribution at gate voltage $V_g = 2.0V$ with no bias voltage. In our fully 3D atomistic quantum mechanical model, we solved self-consistently the 3D Poisson equation (1) for electrostatic potential $\phi(\mathbf{r})$ and exact 3D Schrödinger equation (2):

$$\nabla[\varepsilon(\boldsymbol{r})\nabla\phi(\boldsymbol{r})] = -4\pi[p(\boldsymbol{r}) - n(\boldsymbol{r}) + N_d^+(\boldsymbol{r}) - N_a^-(\boldsymbol{r})] \quad (1)$$

$$(-\frac{1}{2}\nabla^2 + V(\boldsymbol{r}) + V_{str}(\boldsymbol{r}) + V_{ext}(\boldsymbol{r}))\psi_i(\boldsymbol{r}) = E_i\psi_i(\boldsymbol{r}) \quad (2)$$

Here $n(r)$ is the occupied electron carrier density to be determined by the electron wavefunction, $p(r)$ is a small hole density calculated by local equation of state, $N_d^+(r)$ is the donate nuclear charge density, and $N_a^-(r)$ is the acceptor nuclear charge density. In our simulation, we have set $N_d^+(r)$ to be zero, i.e., no donor. In our previous simulation, $N_a^-(r)$ is treated as an continuous function, thus, there were no individual dopant atoms. In the present work, we have chosen the individual acceptor position $\{R_j\}$ randomly according to the average doping concentration. In average, there are 169 dopant atoms in the simulated region. No dopant-dopant position correlation is assumed. Then the acceptor nuclear charge at a given temperature T is:

$$N_a^-(r) = \sum_j (\frac{2\pi}{a})^3 e^{-(r-R_j)^2/a^2} \frac{1}{e^{(E_b-\phi(r)-E_f)/kT}+1} \quad (3)$$

here E_b is the donor binding energy position, and E_f is the Fermi energy. We have used an finite $a = 0.3nm$ to represent the effective donor nuclear charge and to make the numerical solution stable. But our results do not depend sensitively on the value of a. The Boltzman factor $\frac{1}{e^{-(E_b-\phi(r)-E_f)/kT}+1}$ represents the occupation probability of an acceptor. Near the channel, for the gate voltage we are considering, almost all the acceptor are occupied, thus the Boltzman factor $\frac{1}{e^{(E_b-\phi(r)-E_f)/kT}+1}$ is almost one, and similarly the hole density $p(r)$ is negligible. $V(\boldsymbol{r})$ in Eq.(2) is a direct sum of the EPM pseudopotential of each atom. $V_{str}(\boldsymbol{r})$ is a confinement potential representing the goemetry and the SiO_2 layer of the device. The additional self-consistent electrostatic potential $V_{ext}(r) = \phi$ is solved from Poisson Equation (1). We have used LCBB[10,11] method to calculate the eigenstates $\{\psi_i(\mathbf{r}), E_i\}$. The LCBB method expands the device wavefunction $\psi_i(\mathbf{r})$ with the bulk Bloch state wavefunctions. We have used 2 conduction band states at each k-points, and k-points around the 6 X-point valleys as our expansion basis to represent $\psi_i(\mathbf{r})$. In a typical calculation, this amounts to 8810 basis functions. To calculate the potential $\phi(r)$ selfconsistently, we have calculated the carrier charge density $n(\mathbf{r})$ from carrier wavefunctions $\psi_i(\mathbf{r})$ as:

$$n(r) = \sum_i 2|\psi_i(r)|^2 \frac{1}{e^{(E_i-E_f)/kT}+1}. \quad (4)$$

In the current study, to simplify the situation, we have used a zero bias between the source and drain. As a result, there is only a single Fermi energy E_f, determined from the source/drain potential. Eqs (1)-(4) were solved self consistently until convergence is achieved using a Pulay DIIS potential mixing iteration scheme [16] to update the potential in Eq(2). Dirichlet and Neumann boundary conditions were used to solve the Poisson eq(1). Further details of our calculation procedure can be found in [9].

III. Results and Discussion

A comparison of the total mobile charge density versus gate voltage for different doping schemes and different simulation approaches is shown in Fig.2. The total mobile charge density Q is just an integral of $n(r)$. To compare with the uniform continuous doping model, we have chosen a random doping configuration for our "atomistic" doping case. The same configuration is used for our quantum mechanical calculation and a semi-classical calculation. In the semi-classical calculation, the coupled drift diffusion and Poisson equations are solved

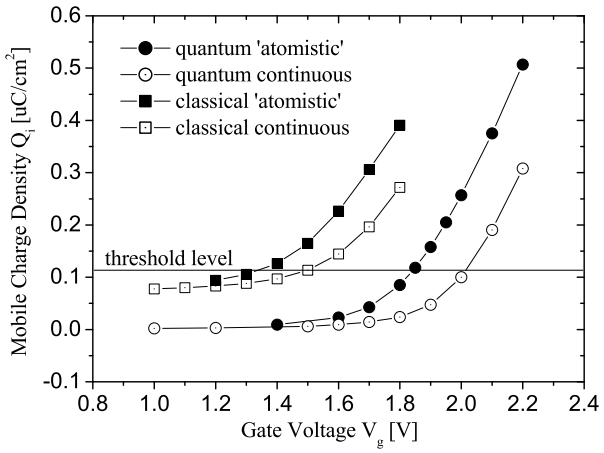

Fig. 2. Comparison of mobile charge density between quantum mechanical calculation and semi-classical calculation. The 'atomistic' curves refer to the same discrete doping case.

selfconsistent without using the gradient correction for the quantum mechanical effects. This is equivalent to calculate the carrier charge density $n(r)$ at a given point $\mathbf{r}$ based on the local potential $\phi(r)$ and the Fermi energy E_f using the Fermi-Dirac distribution.

By comparing the continuous doping result with the atomistic doping result, we see that the gate voltage threshold has been decreased by about 0.15 V due to the atomistic nature of the doping. This is roughly true for both quantum mechanical simulation and the classical simulation, although this lowering is slightly larger in the quantum mechanical simulation, for this particular dopant configuration. Comparing with the classical simulation result, the quantum mechanical threshold voltage is about 0.4 V higher, as found in our previous calculations [9]. The lowering of the gate voltage in the atomistic doping case is due to some local potential minimum (valley) which holds carrier charge density before the average potential reach the carrier inversion threshold. Such local carrier density can form percolation to conduct current [13]. To illustrate the carrier density in real space, we have shown in Fig.3 the cross section perpendicular to the gate substrate and along the channel direction. One can see that, in the atomistic doping case, there is a lump of charge in the middle of the channel due to a local potential minimum at that spot. Such local charge reduces the threshold of the carrier inversion. In Fig.3, we also show the selfconsistent potential for the continuous doping case and the atomistic doping case. We see that, corresponding to the charge density lump, there is a potential minimum at that place.

The biggest difference between the quantum mechanical simulaiton and the semi-classical simulation is the average distance of the occupied electron charge density to the Si-SiO_2 interface. This is due to the quantum confinement effects as discussed in [9]. One can calculate the center of mass of $n(r)$ (charge centroid) and plot its position versus the applied gate voltage. The results are shown in Fig.4 for our

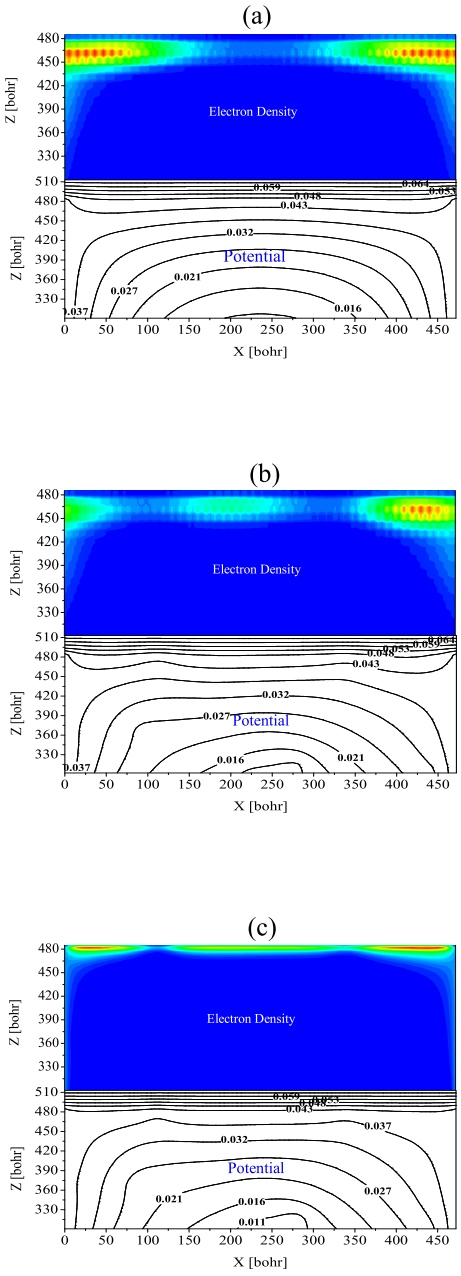

Fig. 3. Mobile Charge Density and Selfconsistently Solved Electrostatic Potential Comparisons on Y Section. Subfigure (a) is for the quantum simulation of continuous doping case, subfigure (b) is for quantum simulation of discrete doping case, and subfigure (c) is for classical simulation of discrete doping case. These figures refer to the middle cross section perpendicular to $Si - SiO_2$ surface and parallel to the source-drain direction.

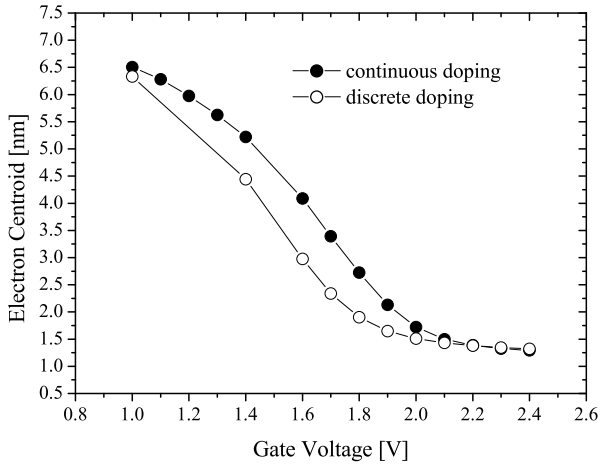

Fig. 4. Comparisons of the inversion layer centroid versus gate voltage, from quantum mechanical simulations.

quantum mechanical simulation. As expected, as the applied gate voltage increase, the charge centroid is more close to the Si-SiO_2 interface. At the end, it saturated at about 1nm away from the Si-SiO_2 interface. What interesting is that the atomistic doping case has a closer charge centroid to the Si-SiO_2 interface than the continuous uniform doping case. This is again probably because there could be some local potential minimum close to the Si-SiO_2 which host some occupied electron charge.

In the above, we only presented one atomistic doping configuration. To get an statistical averaging, we have carried out both quantum mechanical and semi-classical simulations for nineteen different individual configurations. The average threshold lowering ($\Delta V_{th}(V)$) is shown in Table I. Here we see that the average lowering is smaller than that shown in Fig.2. This is because that, in Fig.2, we chose one of the nineteen configurations which has the most severe threshold lowering to highlight discrete dopant induced effect. Although the threshold lowerings of quantum and classical simulations seem to be comparable, the averaged threshold lowerings shown in TABLE.I. are different for these two simulations. We see that, the lowering due to random dopant distribution in quantum mechanical simulation is smaller than in semi-classical simulation. This is probably because in quantum mechanical simulation, due to quantum confinement effect, the electron cannot occupy some narrow potential local minimum, while they can do that in semi-classical simulation. Thus, in the semi-classical simulation, the electron can take the full advantage of the local potential minimum effects, while such effects have been smeared out in some degree in quantum simulation by quantum confinement effect. This explains why semi-classical simulation has a larger threshold reduction.

With the nineteen different simulations, we can calculate the threshold fluctuation as $\sigma V_{th} = [\sum_{j=1,N}(V_{th,j} - V_{th,ave})^2/(N-1)]^{1/2}$**.** The results are also listed in Table I. According to the above argument of quantum confinement effect smearing out the potential local minimum effects, one might think the fluctuation in the quantum mechanical case should be smaller than the classical case. **That is just opposite of what is shown in Table I, where the 0.04552 V quantum mechanical fluctuation is 15.2% larger than the 0.03952 V semi-classical fluctuation.** This increase of the threshold fluctuation due to quantum mechanical effects has also been found in density gradient method [13]. This seemly puzzling phenomina can be explained by the following due to another quantum mechanical effect. In the quantum simulation, the average charge density is away from the Si-SiO_2 interface as shown in Fig.3 and Fig.4. This is equivalent to having a larger SiO_2 layer in the semi-classical simulation. The threshold fluctuation however has an direct relationship to the SiO_2 thickness. For small SiO_2 thickness, the potential near the Si-SiO_2 interface (where the carrier charge is) is pinned by the gate potential. Thus, the randomness of the acceptor positions plays a small role in determining the potential at the inteface (hence the random fluctuation of the threshold is small). Thus, for quantum simulation, where the effective charge distance to the gate substrat is large, the fluctuation is also large. To test this hypothesis more quantitatively, we have taken the electron charge centroid z_i (measure from the Si-SiO_2 interface) near the threshold gate voltage of $V_g = 2V$, and convert that into effective extra SiO_2 thickness as $\triangle = \varepsilon_{ox} z_i/\varepsilon_{Si}$ [14]. We have done three different semi-classical simulations using this $\triangle$ to test different effects of this phenomina.

First, we have used an average $\triangle = 0.6nm$ from the quantum mechancial z_i for all the configuration cases, then we repeat the semi-classical calculations for all the previous individual configurations, and recalculate the average threshold ΔV_{th} and threshold fluctuation σV_{th}. The results are listed in the fourth row of Table.I. We can see that the threshold lowering with this simulation (from the classical continuous model with $t_{OX} = 2.1nm$) is much larger than the quantum mechanical simulaiton result. This indicate that this effective increase of t_{OX} cannot be used to explain the small ΔV_{th} of quantum mechanical calculation compared to semi-classical calculation. On the other hand, the threshold fluctuation σV_{th} of this classical simulation agree perfectly with the quantum mechanical result.

In above, we have used an average $\triangle$. However, there is also an fluctuation of $\triangle$ among different dopant configurations, in the range of 0.5258 nm to 0.6363 nm. To investigate the effect of this fluctuation, we have done semi-classical simulation for each configuration with its own $\triangle$ from the corresponding quantum mechanical simulation. The results are shown in row 5 of Table I. As one can see, the results are essentially the same as in row 4 where this $\triangle$ fluctuation is ignored. To further confirm that the effect of $\triangle$ fluctuation is small, we have done semi-classical simulations with uniform continuous doping profile while using the different $\triangle$ for different individual doping configurations from the quantum mechanical simulation. The results are shown in row 6 of Table I. This time, the threshold fluctuation is extremely small, indicating that the effective thickness fluctuation doesn't play a role. Instead, the increase fluctuation of the quantum mechanical simulation is purely due to the increased average distance of the carrier

TABLE I

GATE THRESHOLD LOWERING $\Delta V_{th}(\Delta V_{th} = V_{th}^{uniformdoping} - V_{th}^{discretedoping})$ AND GATE THRESHOLD FLUCTUATION σV_{th} FROM DIFFERENT SIMULATION METHODS. FOR ROW 5, THE ΔV_{th} IS MEASURED FROM CLASSICAL SIMULATION OF UNIFORM CONTINUOUS DOPING WITH CORRESPONDING FLUCTUATED t_{OX}.

model	quantum 'atomistic'	classical 'atomistic'	classical 'atomistic'	classical 'atomistic'	classical 'continuous'
$t_{ox}(nm)$	1.5	1.5	2.1	1.5+$\Delta^{fluctuated}$	1.5+$\Delta^{fluctuated}$
$\Delta V_{th}(V)$ **01**	0.05566	0.065	0.09984	0.10213	—
$\Delta V_{th}(V)$ **02**	-0.00172	0.05125	0.06333	0.06744	—
$\Delta V_{th}(V)$ **03**	0.08472	0.07096	0.06239	0.06216	—
$\Delta V_{th}(V)$ **04**	0.09277	0.07071	0.07771	0.07959	—
$\Delta V_{th}(V)$ **05**	0.07144	0.13389	0.19347	0.19265	—
$\Delta V_{th}(V)$ **06**	0.06005	0.08073	0.0773	0.0745	—
$\Delta V_{th}(V)$ **07**	0.05666	0.09808	0.12219	0.12427	—
$\Delta V_{th}(V)$ **08**	0.06473	0.07354	0.08262	0.07988	—
$\Delta V_{th}(V)$ **09**	0.06036	0.07597	0.12034	0.12005	—
$\Delta V_{th}(V)$ **10**	0.08653	0.12169	0.16308	0.16313	—
$\Delta V_{th}(V)$ **11**	0.03646	0.04056	0.10271	0.10466	—
$\Delta V_{th}(V)$ **12**	-0.00905	0.05906	0.06227	0.06465	—
$\Delta V_{th}(V)$ **13**	-0.01508	-0.00425	0.01042	0.00472	—
$\Delta V_{th}(V)$ **14**	0.18534	0.16087	0.17156	0.17191	—
$\Delta V_{th}(V)$ **15**	-0.00203	0.0599	0.05617	0.05798	—
$\Delta V_{th}(V)$ **16**	0.06877	0.14914	0.16084	0.16207	—
$\Delta V_{th}(V)$ **17**	0.03134	0.05942	0.05289	0.05201	—
$\Delta V_{th}(V)$ **18**	0.05601	0.09512	0.09225	0.0938	—
$\Delta V_{th}(V)$ **19**	0.05707	0.10239	0.11767	0.11878	—
average $\Delta V_{th}(V)$	0.05474	0.08232	0.09942	0.09981	—
$\sigma V_{th}(V)$	0.04552	0.03952	0.04742	0.04794	0.00239

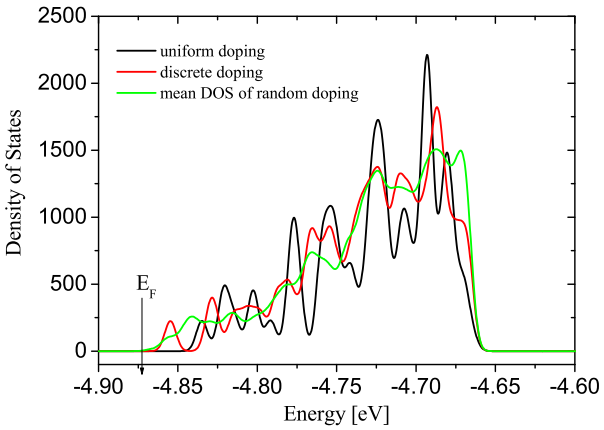

Fig. 5. Density of states comparison between continuous doping and discrete doping. Both cases are at gate voltage $V_g = 2.0V$ with no bias. The averaged density of states is also shown here. The downward arrow shows the Fermi energy.

charge to the Si-SiO_2 interface. In summary, comparing to semi-classical simulation, the decrease in quantum mechanical simulation for average threshold lowering ΔV_{th} from the uniform continuous doping case is due to quantum smearing of the local potential minimum effects, while the increase of the threshold fluctuation is due to the increased distance of the carrier charge density to the Si-SiO_2 interface.

Our fully 3D quantum mechanical model enables us to study the details of quantum mechanical effects, such as the electron density of states. Fig.5 compares the density of states between continuous doping case and the one discrete doping case of Fig.2, Fig.3, and Fig.4. Fig.5 also shows the average density of states of the nineteen different configurations. Two major features can be seen from Fig.5. First, the discrete doping case possesses a smoother density of states. Second, the discrete dopant shift the tail of the density of states lower toward the Fermi energy E_F. In the continuous doping case, the potential is symmetric and uniform in the z direction of Fig.1. Due to these symmetry, there are degeneracy of the eigenstates, and the density of state shows big peak structures. A random dopant configuration and its corresponding random potential destroy these symmetries, thus result in an overall smoother DOS. The down shifting of the DOS in the discrete dopant case is due to local potential minimum. This DOS down shifting corroborates well with the lowering of the gate threshold voltage.

IV. CONCLUSION

In this paper, we have presented fully 3D quantum mechanical atomistic simulations to study the random dopant induced effects such as threshold fluctuation and lowering. We solved single particle wavefunctions $\{\psi_i(\mathbf{r}), E_i\}$ from the empirical pseudopotential Schrödinger equation using LCBB method and calculated the occupied carrier charge density from these wavefunctions. This is then coupled with the Poisson equation to form a self-consistent simulation. Our results show a 15.2% larger threshold fluctuation of the quantum mechanical simulation than that of semi-classical method, while a smaller threshold lower than the semi-classical result. We found that the smaller threshold lower is due to effective smearing of the potential local minimum due to quantum confinement effect, while the increase threshold fluctuation is due to increase distance of the carrier charge density to the Si-SiO_2 interface (as a result, the potential in the large carrier charge density

area cannot be pinned down by the gate potential). Thus, unfortunately, quantum mechanical effect does not reduce the gate threshold random fluctuation, instead it exacerbates the problem. This finding for the threshold fluctuation is qualitatively similar to the previous study using approximated density gradient method to include the quantum mechanical effects [13]. However, our finding for threshold lowering (from the continuous doping case) is opposite from the density gradient method. In the density gradient method, the quantum mechanical lowering is larger than the semiclassical lower [13], while in our simulation, the quantum mechanical lowering is smaller than the semiclassical results. This highlight the needs for accurate and direct quantum mechanical simulations.

ACKNOWLEDGMENT

This work is supported by the National Natural Science Foundation of China (Grant No.60521001 and 60776061). The work by L.W.W is also funded by the U.S. Department of Energy BES, office of science, under Contract No. DE-AC02-05CH11231.

REFERENCES

[1] International Technology Roadmap for Semiconductors. Available at http://public.itrs.net.
[2] M. Ieong, B. Doris, J. Kedzierski, K, Rim, and M. Yang, ”Silicon Device Scaling to the Sub-10-nm Regime,” Science vol.306, pp.2057-2060, 2004.
[3] Y. Taur, ”CMOS design near the limit of scaling,” IBM J. RES. & DEV. vol.46, no.2/3, pp.213-221, 2002.
[4] T. Hiramoto, M. Saitoh and G. Tsutsui, ”Emerging nanoscale silicon devices taking advantage of nanostructure physics,” IBM J. RES. & DEV. vol. 50, no. 4/5, pp.411-417, 2006.
[5] H. Iwai, ”CMOS downsizing toward sub-10 nm,” Solid-State Electronics, vol.48, pp.497-503, 2004.
[6] Scott Roy and Asen Asenov, ”Where Do the Dopants Go?” Science vol.309, pp.388-390, 2005.
[7] Daniel Connelly, Zhiping Yu, and Dan Yergeau, ”Macroscopic Simulation of Quantum Mechanical Effects in 2-D MOS Devices via the Density Gradient Mechod,” IEEE Trans, Electron Dev, vol.49, no.4, pp.619-626, 2002.
[8] Agostino Pirovano, Andrea L. Lacaita, and Allessandro S. Spinelli, ”Two-Dimentional Quantum Effects in Nanoscale MOSFETs,” IEEE Trans, Electron Dev, vol.49, no.1, pp.25-31, 2002.
[9] Jun-Wei Luo, Shu-Shen Li, Jian-Bai Xia and Lin-Wang Wang, ”Quantum mechanical effects in nanometer field effect transistors,” Appl. Phys. Lett vol.90, pp.143108, 2007.
[10] L. W. Wang and A. Zunger, ”Linear combination of bulk bands method for large-scale electronic structure caculations on strained nanostructures,” Phys. Rev. B, vol.59, pp.15806-15818, 1999.
[11] J. W. Luo, S. S. Li, J. B. Xia, and L. W. Wang, ”Comparative study for colloidal quantum dot conduction band state calculations,” Appl. Phys. Lett, vol.88, pp.143108, 2006.
[12] B. Hoeneisen, C. A. Mead, ”Limitations in microelectronics ł II. Bipolar technology ,” Solid State Electronics, vol.15, pp.891-897, 1972.
[13] Asen Asenov, Gabriela Slavcheva, Andrew R. Brown, John H. Davies, and Subhash Saini, ”Increase in the Random Dopant Induced Threshold Fluctuations and Lowering in Sub-100 nm MOSFETs Due to Quantum Effects: A 3-D Density-Gradient Simulation Study,” IEEE Trans, Electron Dev, vol.48, no.4, pp.722-729, 2001.
[14] M. G. Ancona and G. I. Iafrate, ”Quantum correlation to the equation of state of an electron gas in a semiconductor,” Phys. Rev. B, vol.39, pp.9536-9540, 1989.
[15] M. G. Ancona and H. F. Tiersten, ”Macroscopic physics of the silicon inversion layer,” Phys. Rev. B, vol.35, pp.7959-7965, 1987.
[16] G. Kresse and J. Furthmuller, ”Efficient iterative schemes for ab initio total-energy calculations using a plane-wave basis set,” Phys. Rev. B, vol.54, pp.11169, 1996.

Xiang-Wei Jiang photograph and biography not available at time of publication.

Hui-Xiong Deng photograph and biography not available at time of publication.

Jun-Wei Luo photograph and biography not available at time of publication.

Shu-Shen Li photograph and biography not available at time of publication.

Jian-Bai Xia photograph and biography not available at time of publication.

Lin-Wang Wang photograph and biography not available at time of publication.